Preparation of Sand Beds Using Fluidization

Preprint · June 2019

DOI: 10.31224/osf.io/u78t9

4 authors:

Zhefei Jin
Northwestern University
6 PUBLICATIONS **111** CITATIONS
SEE PROFILE

Junyue Tang
Harbin Institute of Technology
23 PUBLICATIONS **174** CITATIONS
SEE PROFILE

Paul Umbanhowar
Northwestern University
163 PUBLICATIONS **5,297** CITATIONS
SEE PROFILE

James P Hambleton
Northwestern University
59 PUBLICATIONS **583** CITATIONS
SEE PROFILE

NORTHWESTERN
UNIVERSITY

Center for Sustainable Engineering of Geological and Infrastructure Materials (SEGIM)

Department of Civil and Environmental Engineering

McCormick School of Engineering and Applied Science

Evanston, Illinois 60208, USA

Preparation of Sand Beds Using Fluidization

Z. Jin, J. Tang, P.B. Umbanhowar, J.P. Hambleton

SEGIM INTERNAL REPORT No. 19-6/039P

June 2019

Preparation of Sand Beds Using Fluidization

Zhefei Jin[a], Junyue Tang[b], Paul B. Umbanhowar[c], James Hambleton[a,*]

[a]*Department of Civil and Environmental Engineering, Northwestern University, Evanston, IL 60208, U.S.A*

[b]*State Key Laboratory of Robotics and System, Harbin Institute of Technology, Harbin, 150001, P.R. China*

[c]*Department of Mechanical Engineering, Northwestern University, Evanston, Illinois 60208, U.S.A*

Abstract

Reconstituting soil beds to a desired density is essential to geotechnical modeling tests. In this study, we apply and assess the method of air fluidization to prepare sand beds for geotechnical engineering studies. Through it, an automated bed preparation process can be realized. The details of device structure and design are presented as a reference for application of the methodology. By quantifying the average and local post-fluidization density of the bed, the performance of the fluidized bed device is characterized. With the addition of vibration and by changing the defluidization rate, the sand can be prepared with volume-based relative densities ranging from 10% to 92%. Local sand density, measured with a cone penetrometer, is nearly uniform across the bed: density variation is less than 13% (COV_{D_r}) for all protocols except for some beds prepared by defluidization only. The variation of local density and penetration resistance measured across the bed breadth is comparable to results from beds prepared by the commonly used method of pluviation. This suggests that sand beds reconstituted using air fluidization are suitable for geotechnical modeling tests.

Keywords: Fluidization; Fluidized bed; Preparation of sand beds; Density variation; Cone penetration; Penetrometer

*Corresponding author

Email addresses: ZhefeiJin2015@u.northwestern.edu (Zhefei Jin), junyue.tang@northwestern.edu (Junyue Tang), umbanhowar@northwestern.edu (Paul B. Umbanhowar), jphambleton@northwestern.edu (James Hambleton), jphambleton@northwestern.edu (James Hambleton)

1. Introduction

Relative density, defined as the ratio of the difference between the void ratios of a cohesionless soil in its loosest state and existing natural state to the difference between its void ratio in the loosest and densest states, significantly influences soil behaviour. In the laboratory, preparation of large soil samples to a required density is a fundamental step in investigating geotechnical problems. For example, [1] studied geosynthetic-soil interaction by performing pull-out tests in a 1.5 m by 0.6 m soil bed; [2] studied the response of footings under planar loading in sand prepared in a cylindrical tank 0.45 m high and with a 0.45 m inner diameter. Traditionally, the reconstitution of dry sand samples is achieved by tamping, vibration and different types of pluviation. These methods are differentiated into two groups: for tamping and vibration, the density of the sample is adjusted after deposition; while for pluviation the density is determined during deposition [3].

With tamping, sand is poured in several layers with each layer compressed by a compactor. Using this method, [4] obtained dry sand samples for triaxial tests with relative density ranging from 40% to 90%. [5] achieved an approximately homogeneous sample with relative densities of 40% and 75% with a 2 m $\times$ 0.6 m sand bed. [6] investigated the influence of tamped layers and compactor drop height on the void ratio and found that neither increasing the number of layers from three to five nor increasing the drop height from 20 mm to 50 mm significantly altered the void ratio. The main drawbacks of tamping are particle crushing during compaction, low repeatability, and relatively pronounced density variation along the depth [7].

Vibration is generally used to prepare medium to dense sand samples. The sample is first prepared in a loose state, and then vibrated under a small amount of surcharge provided by a cap. [8] and [9] successfully used this method to prepare dense sand samples for 1 g laboratory and higher g centrifuge tests, respectively. By monitoring subsidence of the cap, [10] obtained specimens with relative densities ranging from 50% to 90% while controlling the percentage error between actual and desired density to less

than 1%.

Compared with tamping and vibration, pluviation in air is used more broadly because of its advantages of reduced segregation, lack of particle crushing, and better repeatability [11]. Studies of air pluviation indicate that relative densities achieved by this method generally range from 40% to 100% [12, 11, 13, 3, 14]. For a given type of sand, the main factors affecting the relative density are the particle drop height, deposition intensity, and the mesh size of the grid through which the sand particles are dropped [15, 16]. A higher drop height leads to a larger fall velocity which increases packing density. This densification is effective for drop height below a certain maximum, since the particle velocity plateaus at larger drop heights due to air drag [17]. For a given drop height, increased deposition intensity decreases deposition density [18, 19, 20], since the simultaneous fall of many particles increases inter-particle interference [13]. Increased deposition intensity can be achieved by increasing the mesh size of the grid [18].

Even though air pluviation is widely used to prepare sand samples in the laboratory, it has some limitations. First, air pluviation is usually not fully automated, which costs time and manpower as sand initially inside the bed needs to be emptied and then poured in again. Second, uniform low density ($\leq 30\%$) samples are hard to achieve, making pluviation more applicable to studies of medium or dense sand packings. Third, the surface of a pluviation reconstituted sample is typically uneven, requiring levelling by post-deposition vacuuming, which is time consuming and can disturb the sample.

Air fluidization can overcome the limitations of the three techniques for reconstituting a sand bed described above. The process of fluidization is similar to liquefaction in which granular material is converted from a static solid-like state to a dynamic fluid-like state when a fluid (liquid or gas) flows upward through the granular material. Fluidization is widely used in the chemical processing industry for separations, heat transfer operations, and catalytic reactions. Recently, Goldman and co-workers used air-fluidization to reconstitute granular material beds [21, 22, 23, 24, 25, 26]. They found that a fluidized bed allows control of the relative density and creation of re-

peatable homogeneous granular bed states, which were typically composed of $\sim 1\,\mathrm{mm}$ poppy seeds. Beds prepared in this way exhibit a spatially uniform penetration resistance that is highly repeatable. In one process, the bed of particles is reconstituted by fluidization and then settled by defluidization. Different degrees of compaction can be achieved by changing the defluidization rate [27]. The dense packing state is realized by slow defluidization while the loose packing state is obtained with rapid defluidization. Generally, varying the defluidization rate is sufficient to prepare samples with loose to medium packing states. Samples can be densified by other techniques, such as vibration. X-ray absorption measurements confirmed that vertical density variations in samples prepared using this technique are small, with less than 0.004 variation in the packing fraction, which is calculated by dividing the total grain mass by the bed volume and the particle density [27].

The objectives of this study are to (1) provide details about using air-fluidization to reconstitute sand beds; (2) characterize physical properties of sand beds created using this technique; and (3) demonstrate the qualification of this method for preparing sand beds for geotechnical modeling tests. To do so, we explain the mechanism of fluidization and describe the design of a fluidized bed device. Through a discussion, we illustrate its potential for use in different types of geotechnical modeling tests with various demands on sand bed soil properties and size. In this study, we use three operating modes: defluidization only (DO), defluidization followed by vibration (DFV) and defluidization concurrent with vibration (DCV) to prepare sand beds with a broad range of relative density (10.4% to 91.7%). For each sand bed, we characterize the density globally and locally by volume-based and penetration-based measurements, respectively. The variation of local density and penetration resistance measured across beds are compared to results from beds prepared by pluviation, a widely used method in geotechnical modeling tests.

2. Fluidized bed device

2.1. Fundamentals of fluidization

In a gas-fluidized bed, the fluidization behaviour differs depending on the superficial gas velocity and particle properties [28, 29]. When gas flow is introduced through the porous bottom of a bed of particles, it moves upwards through voids between particles. At low gas velocities, the drag force exerted on each particle is low, resulting in a static bed. As the gas velocity is increased, the drag force begins to counteract the gravitational force, causing the bed to expand in volume as the particles move away from each other. With further increase in the gas velocity, a critical value is reached at which the upward drag force equals the downward gravitational force, causing the particles to become suspended. At this critical value, the bed is said to be fluidized and exhibits fluid behaviour in that it can no longer support internal stresses. With further increases in the gas velocity, the bed begins to bubble. The bulk density of the bed continues to decrease, and the fluidization becomes more violent until particles no longer form a bed but are "conveyed" upwards by the gas flow. Stopping the gas flow causes the particle bed to defluidize in three consecutive stages: a rapid initial stage for bubble escape, an intermediate stage of hindered sedimentation with a constant velocity of solids descent, and a final decelerating stage of solids consolidation [30].

Not all particle beds undergo the full process of fluidization and defluidization described above. The specific behavior depends on particle properties, primarily size and density. Based on particle size and density, Geldart categorize particles into Groups A-D [28, 29]. Group A designates aeratable particles. These materials (e.g., milk flour) normally have a small mean particle size and/or low particle density. Beds of these particles can be fluidized at low gas velocities without the formation of bubbles and are subject to the full fluidization-defluidization process. Group B particles form bubbling beds. Most have particles with size between 150 μm and 500 μm and density from about 1.4 to 4 g/cm^3. For these particle beds, once the minimum fluidization velocity is exceeded, the excess gas appears in the form of bubbles; in the defluidization process,

the particle beds reach their final state as soon as bubbles are expelled [30]. Group C particles are cohesive or very fine powders. They are extremely challenging to fluidize and typically exhibit channeling in which gas flow is concentrated in a number of discrete "holes" in the bed. Group D particles form spouting beds and are composed of very large or very dense particles, such as coffee beans and wheat. As the gas velocity is increased, a jet forms in the bed, and the material may potentially be blown out of the bed. In this paper, we use silica sand which is a Group B particle.

Before discussing the design of the fluidized bed device, we review the airflow requirements to achieve particle fluidization. As stated above, the inception of fluidization is triggered when the air velocity reaches a value at which the upward drag forces on the particles equals the downward gravitational force. Considering the entire bed, this force balance condition occurs when the product of the flow induced pressure drop across the bed and the bed cross-sectional area equals the weight of the soil in the bed [31]. The pressure drop across the bed depends on the air velocity, and it has been investigated and described by various models [32, 33, 31, 34]. To illustrate the general approach, we characterize the relationship between the pressure drop across the bed ΔP and the superficial airspeed v (calculated as Q/A, where Q is the volumetric air flow rate and A is the cross-sectional bed area) using Erguns equation:

$$\frac{\Delta P}{L} = \frac{150\mu(1-\epsilon)^2 v}{d^2\epsilon^3} + 1.75\frac{1-\epsilon}{\epsilon^3}\frac{\rho_a v^2}{d}, \tag{1}$$

where L is the particle bed height; μ is the dynamic viscosity of the fluidizing gas; ρ_a is the gas density; d is the average grain diameter; and ϵ is the bed porosity. The left-hand side of Eq. (1) equals the unit weight of the particle bed (γ_b). By transforming γ_b to the unit weight of a grain (γ_g) with the relation $\gamma_b = \gamma_g(1-\epsilon)$, the minimum required flow rate (Q_{mf}) for fluidization can be calculated from:

$$\gamma_g = \frac{150\mu(1-\epsilon)Q_{mf}}{d^2\epsilon^3 A} + 1.75\frac{\rho_a Q_{mf}^2}{d\epsilon^3 A^2}. \tag{2}$$

2.2. Design of the fluidized bed device

In principle, a flow of air at the minimum required flow rate (Q_{mf}) is required to achieve fluidization; however, in practice, a facility is needed to provide the required

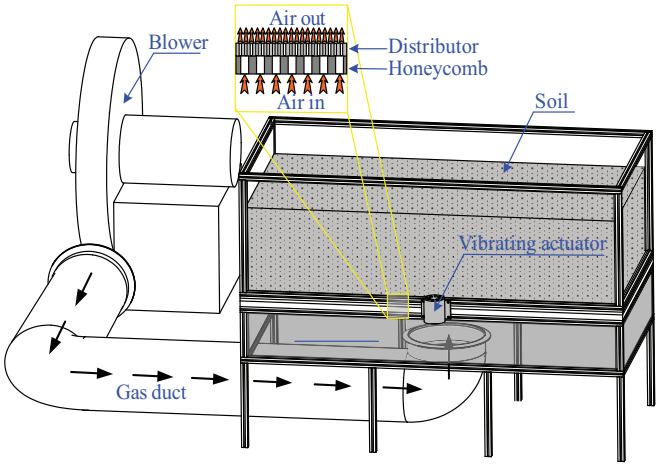

Figure 1: Schematic diagram of fluidized bed apparatus.

airflow. Fig. 1 is a model diagram of our 150 cm (length) × 75 cm (width) × 50 cm (height) fluidized bed located in the Soil-Structure and Soil-Machine Interaction Laboratory (SSI-SMI Laboratory) at Northwestern University. A 10 hp centrifugal fan blower with three-phase motor (Chicago Blower Corp.) produces the required flow of high-pressure air, which is transmitted by a duct to the plenum. The 20 cm tall plenum pre-distributes the air, and its walls are 1.8 cm thick acrylic recessed in the extruded aluminum rails (80/20 Inc.) which form the frame of the box. At the top of the plenum is a 2.54 cm thick layer of steel honeycomb for structural rigidity and flow distribution. Above the honeycomb, a 1.27 cm thick layer of porous plastic with 20 μm pores (GenPore) forms the distributor. The distributor supports the particles in the bed, and, more importantly, promotes the uniform flow of air through the particle bed. The extra vertical space above the sand surface and below the top of the container box helps to contain the sand. The blower is driven by a variable frequency drive controller (model #CFW110028T2ON1Z, WEG), which supports proportional voltage control of the fan speed. The 0-10 V fan speed control signal comes from a USB 6001 DAQ (National Instruments) controlled by a MATLAB program.

To understand the design of the fluidized bed device, we explain how the blower works. Air enters the blower at atmospheric pressure, and then is pressurized by the

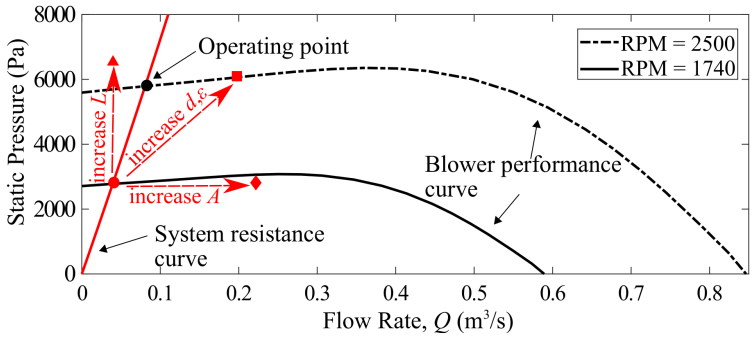

Figure 2: System and blower curves for fluidized bed device. The intersection of the blower and system curves determines the operating point.

blower. This pressure difference drives the air through the duct, plenum, distributor, and bed material. As described in the previous section, to fluidize the particles, the air flow through the bed must reach the minimum required air flow rate (Q_{mf}). The air flow rate in the system is determined not only by the operating motor speed of the blower but also the flow resistance of the entire system. At any fixed motor speed, the blower operates by delivering air flow against a certain static pressure as specified by a "performance curve" such as the one shown in Fig. 2 (the actual performance curve for the blower used in the study). For a system, the static pressure depends on the air flow rate. Therefore, the pressure required by a system over a range of flow rates can be determined, and a "system resistance curve" can be developed and plotted on the blower performance curve to show the blowers actual operating point, i.e., the intersection point. This point moves as the system or the motor speed changes. For example, at a certain motor speed, the operating point is the one with zero flow rate when the system is sealed, and with zero static pressure when the system is totally open. In terms of a given system (such as the one indicated by the red line in Fig. 2), the operating point moves from the red point to the black point as the motor speed is increased from 1740 RPM to 2500 RPM (Revolutions Per Minute). Hence, to fluidize a given bed, a specific motor speed is required corresponding to the minimum required flow rate (Q_{mf}). To obtain this desired operating point, the system resistance curve for the device must be determined.

By design, the largest resistance in a fluidized bed device comes from the distributor and the particle bed. In most cases, the pressure drop for a given flow rate follows a second-order relationship [35]. The pressure drop of the distributor (ΔP_d) is generalized as $\Delta P_d = \frac{m}{A_d^2}Q^2 + \frac{n}{A_d}Q$, where A_d is the area of distributor, which is the same as the cross-sectional area of bed (A); m and n are parameters mainly determined by the hole size, hole number, and the thickness of the porous sheet. For air flowing through the bed of particles, the pressure drop can be calculated from Eq. (1) as $\Delta P_b = \frac{150\mu(1-\epsilon)^2 L}{d^2\epsilon^3 A}Q + 1.75\frac{1-\epsilon}{\epsilon^3}\frac{\rho_a L}{dA^2}Q^2$. It should be noted that to equally distribute air flow through the bed, a constraint between the minimum distributor pressure drop and the bed pressure drop is imposed, i.e. $\Delta P_d \geq c\Delta P_b$, where c is proposed to range from 0.02 to 1, with 0.3 as a widely quoted value [36, 37]. By combining the pressure drop from the distributor and the bed, the system resistance is characterized as:

$$\Delta P_s = \left(1.75\frac{1-\epsilon}{\epsilon^3}\frac{\rho_a L}{dA^2} + \frac{m}{A^2}\right)Q^2 + \left(\frac{150\mu(1-\epsilon)^2 L}{d^2\epsilon^3 A} + \frac{n}{A}\right)Q. \tag{3}$$

Assigning the value of the minimum required flow rate (Q_{mf}) to the flow rate (Q) in Eq. (3), the desired operating point (Q,P) can be located on the system resistance curve, which determines the desired motor speed.

To validate the design methodology, tests of the fluidized bed in the SSI-SMI lab were performed using silica sand, obtained from Ottawa, Illinois (supplied by U.S. Silica Company) and characterized according to ASTM procedures. Fig. 3 shows the grain-size distribution curve of the sand based on data from the supplier. The particles are round in shape and range in size from 0.075 mm to 0.425 mm with a mean diameter of $D_{50} = 0.19$ mm. Based on the curve, the coefficient of uniformity, C_u, and the coefficient of curvature, C_c, are 1.61 and 1.03, respectively; hence the sand is classified as poorly-graded (SP). The maximum density (ρ_{max}) of this sand is measured as 1730 kg/m^3 [38], and its minimum density (ρ_{min}) is 1450 kg/m^3 [39].

Fig. 2 shows the actual blower performance curves and the estimated system resistance curve. The parameters used to determine the system resistance curve are m = 26808 Pa·s^2/m^2, n = 24488 Pa·s/m, d = 0.19 mm, γ_g = 26 kN/m^3, L = 0.127 m, ϵ =

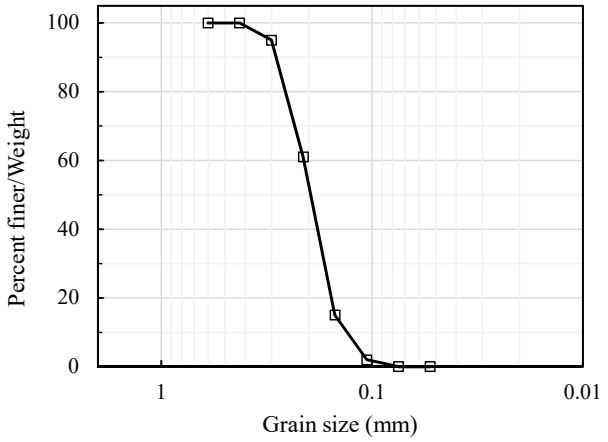

Figure 3: Cumulative grain-size distribution of the silica sand (Ottawa) used in this study (data provided by U.S. Silica).

0.396, $A = 1.125\,\mathrm{m}^2$, $\mu = 1.81 \times 10^{-5}\,\mathrm{kg/m{\cdot}s}$ (at $25\,^{\circ}\mathrm{C}$), $\rho_a = 1.225\,\mathrm{kg/m}^3$. Among these parameters, m and n are obtained based on the information provided by the porous layer manufacturer; d is determined from the grain size data provided by U.S. Silica; γ_g is approximated as the unit weight of quartz, the main mineral component of Ottawa sand; L is the average height of the sand bed measured before the verification test, which can be used to estimate the bulk density of the bed; and ϵ is determined by the sand particle density and the estimated bulk density on the premise that the sand is distributed uniformly. Based on the calculation, the minimum required flow rate and airspeed are $0.04\,\mathrm{m}^3/\mathrm{s}$ and $0.035\,\mathrm{m/s}$, respectively. The pressure drop across the distributor and particle bed at fluidization is predicted to be $2763\,\mathrm{Pa}$, which is close to the actual gauge pressure measured in the plenum of $2922\,\mathrm{Pa}$. According to the above calculation and blower performance curve, the bed of sand should fluidize at a motor speed of $1740\,\mathrm{RPM}$, while the actual value to achieve fluidization is slightly higher at $1780\,\mathrm{RPM}$. The small difference may result from air leaks and the unaccounted for additional resistance from the duct, honeycomb and honeycomb support. Reducing these effects is vital to the efficiency and precise design of the fluidized bed device.

2.3. Fluidized bed device capabilities

The demands on a sand bed for geotechnical model testing vary with the soil properties and bed size. The fluidized bed device can be adjusted to accommodate specific demands, mainly through the selection of the distributor and the operation of the blower. The soil properties affecting the required airflow for achieving fluidization include the unit weight and average diameter of the grains and the soil porosity. Unit weight varies with grain mineral content. Most sand is made of quartz, so the unit weight is generally regarded as constant, i.e., $26\,\mathrm{kN/m^3}$ [40]. Consequently, only the influence of grain diameter and porosity are discussed below. With increase of average grain diameter or porosity of the sand bed, the minimum required flow rate increases, which raises the distributor pressure drop (ΔP_d). However, the bed pressure drop (ΔP_b), which equals the weight of sand per unit area, remains constant. Hence, the desired operating point moves to the position with higher static pressure and flow rate (red square symbol in Fig. 2), which can be reached by increasing the motor speed. Note these desired points in Fig. 2 are plotted to illustrate the influence of different factors on the airflow requirements, and do not correspond to any specific sand bed.

Now we consider the effects of bed size, which refers to the height and the cross-sectional area of the sand bed. The height of the sand bed has no influence on the minimum required flow rate and ΔP_d, while ΔP_b increases linearly. Accordingly, the blower should provide higher pressure with the same flow rate (triangular symbol in Fig. 2 is the new desired operating point). Note that a distributor with higher resistance (higher m, n) might be required in order to guarantee the design constraint $\Delta P_d \geq c\Delta P_b$. Distributor resistance can be increased by increasing its thickness, decreasing the holes size, or decreasing the number of holes. For the fluidized bed in the SSI-SMI lab, the maximum motor speed is 3600 RPM, at which the blower can produce a maximum pressure around 11960 Pa and a maximum flow rate of $0.7\,\mathrm{m^3/s}$. At this speed and with the sand described in the previous section, the maximum depth of the fluidized sand bed is 0.72 m. However, in this case, $\Delta P_b \approx 10812\,\mathrm{Pa}$, and $\Delta P_d \approx 855\,\mathrm{Pa}$, so the constraint between them, i.e. $\Delta P_d \geq c\Delta P_b$ is not satisfied with $c = 0.3$. A higher

resistance distributor can help this condition. The deepest fluidizable sand bed is about 0.61 m for the utilized blower if the ΔP_d reaches 2760 Pa, which can be accomplished by increasing the current distributor thickness to 4.1 cm.

For sand beds with larger cross-sectional areas, the minimum required flow rate increases, while the minimum required airspeed stays the same. According to Eq. (3), system resistance remains constant at constant airspeed. Therefore, a higher flow rate but the same static pressure is needed. Correspondingly, the desired operating point is shifted purely horizontally (red diamond symbol in Fig. 2). When the fluidized bed in the SSI-SMI lab is run at the maximum motor speed, the largest cross-sectional area of the fluidizable bed is about 25 m^2 which limits the maximum sand bed depth to 0.61 m.

3. Sand bed characterization

In this study, sand beds are prepared using three different operating modes: defluidization only (DO), defludization followed by vibration (DFV), and defluidization concurrent with vibration (DCV). In mode DO, the sand settles gradually with decreasing airflow to form the sample. Mode DFV extends the DO method by vibrating the the sand bed after defluidization with the same time of defluidization. Mode DCV vibrates the bed during defluidization. The vibration in the latter two modes is induced by a vibrating motor (Fasco #D1130) attached to the middle of one side of the fluidized bed frame, as shown in Fig. 1. In the tests, 227 kg of sand was placed on the bed with an initial height of 0.130 m. The sand was fully fluidized by increasing the motor speed to 1780 RPM, at which point the pressure in the plenum (P_0) is 2922 Pa. The fully fluidized stage was maintained for 10 s, after which the defluidization stage was started. The motor speed was linearly decreased from 1780 RPM to 0 over a variable defluidization time (T) to reduce the pressure and flow rate of air. For each of the three modes listed above, defluidization times (T) ranging from 50 s (the stopping time of the blower is $\approx$ 40 s) to nearly 10 hrs were applied to reconstitute the sand beds. The volumetric density and local density of the resulting beds were then measured as described below. Note that in addition to vibration, beds also can be densified by short

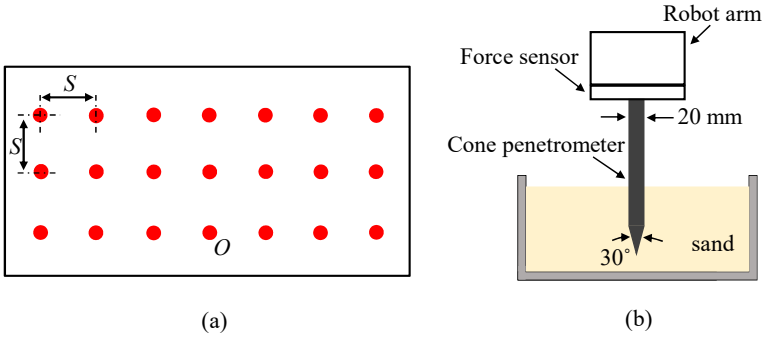

Figure 4: (a) Locations of sand height measurements and penetration tests. (b) Schematic of cone penetration measurement.

periodic air pulses [23].

3.1. Volumetric density

The volume-based density of the bed (ρ_v) is measured as a function of the defluidization time for the three operating modes. To do so, the volume of each reconstituted sand bed is determined with a laser based distance sensor (Leica Disto E7400X) attached to a six-axis ABB IRB-4400 robot, whose movement is controlled automatically by a connected computer. First, the distance to the distributor (empty bed) H_i is measured at 21 positions on a uniform 17.5 cm grid, see Fig. 4(a), as the robot moves the distance sensor in a horizontal plane. Then, after the bed is filled and reconstituted, the distance between the end of the robot arm and the surface of the sand h_i is measured at the same positions. The top of the distributor (bottom of bed) and the reconstituted sand surfaces are nearly flat: H_i varies by less than 0.2 cm and h_i by less than 0.6 cm for all cases. The volume of sand in the bed is then estimated as $V = A(\overline{H_i} - \overline{h_i})$, where A is the bed cross-sectional area and the overline indicates the ensemble average. Assuming that the sand bed is uniform in density, the volume-based density of the sand bed is $\rho_v = M/V$, where M is the mass of sand in the bed, and the corresponding relative density is $D_r = \dfrac{\rho_{max}(\rho_v - \rho_{min})}{\rho_v(\rho_{max} - \rho_{min})}$, where ρ_{max} and ρ_{min} are determined in the section entitled "Design of the fluidized bed device."

The volume-based relative density of the sand bed versus the pressure ramp rate

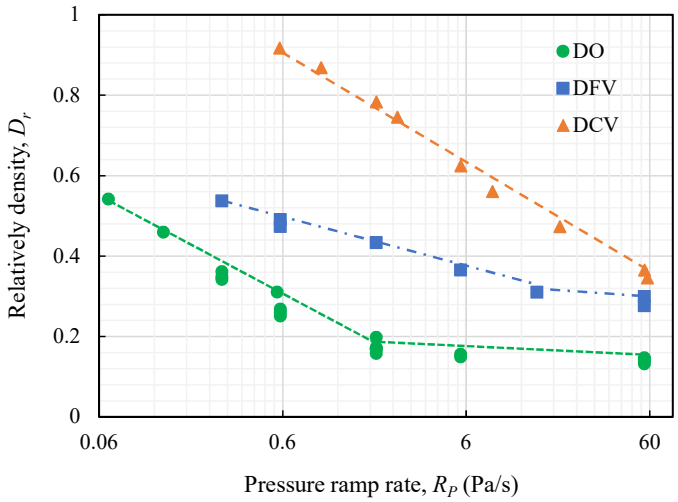

Figure 5: Relative density of sand prepared by defluidization only (DO), defluidization followed by vibration (DFV), and defluidization with concurrent vibration (DCV) for various pressure ramp rates.

$R_p = P_0/T$ increases with decreasing R_p for all cases as shown in Fig. 5. D_r values ranging from 0.9 to nearly 0.1 are realized. The relative density is logarithmic in the pressure ramp rate, and can be written as $D_r = \alpha \log(R_p/\beta)$. Similar scaling was previously reported by [41]. For the DCV mode, a single pair of α and β values fit the data over the entire range of R_p. However, for DO and DFV operating, there are two distinct regions of response. At higher pressure ramp rates, the increase of D_r with decreasing R_p is noticeably weaker than at lower R_p. In addition, at the same pressure ramp rate, the sample prepared by DCV achieves the largest D_r, while the sample prepared using DO has the lowest D_r. Comparing the results obtained from DO and DFV, the effect of vibration is weakened when the pressure ramp rate is less than 2 Pa/s for DFV.

3.2. Local density

3.2.1. Penetration-based density measurement

In addition to volume-based density measurements, local density measurements can be used to characterize the bed homogeneity. To do so, a penetration test was developed as a fast and simple method for acquiring information of *in situ* soil properties. The test

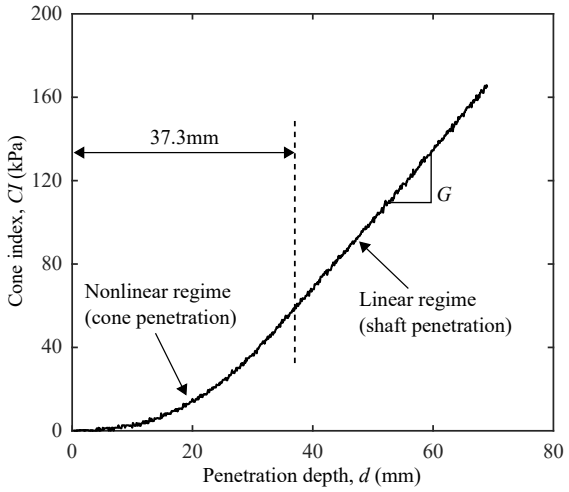

Figure 6: Illustration of a cone index profile (mode DCV with $T = 3000\,\mathrm{s}$), where G is the slope in the shaft penetration regime (see text).

uses the robot arm to drive a penetrometer into the soil at a fixed rate while recording the resisting force with a force sensor. Our penetrometer geometry (30° circular cone tip and a $3.2\,\mathrm{cm}^2$ base) is inspired by a United States Army Corps of Engineers Waterways Experiment Station penetrometer design used to determine soil trafficability [42]. The resistive forces and moments acting on the penetrometer while it interacts with the sand bed are measured by a six-axis load cell (Sunrise Instruments #3314C) installed at the end of the ABB robot arm, as illustrated schematically in Fig. 4(b). The sensor simultaneously measures forces in three mutually perpendicular directions and torques about three corresponding axes, but only the vertical resistive force is used in this study. At each location tested, the cone penetrometer penetrated the soil to a depth of about 80 mm at a speed of 1 mm/s. The cone index (CI) characterizes the penetration resistance [42], and is defined as the force per base area required to penetrate the cone into the soil. A typical cone index profile for dry sand is illustrated in Fig. 6 and consists of two stages: a non-linear with depth cone penetration regime followed by a linear with depth shaft penetration regime.

Previous studies found that factors affecting CI include moisture content, density, and soil type. To illustrate the effects of different defluidization modes and times T,

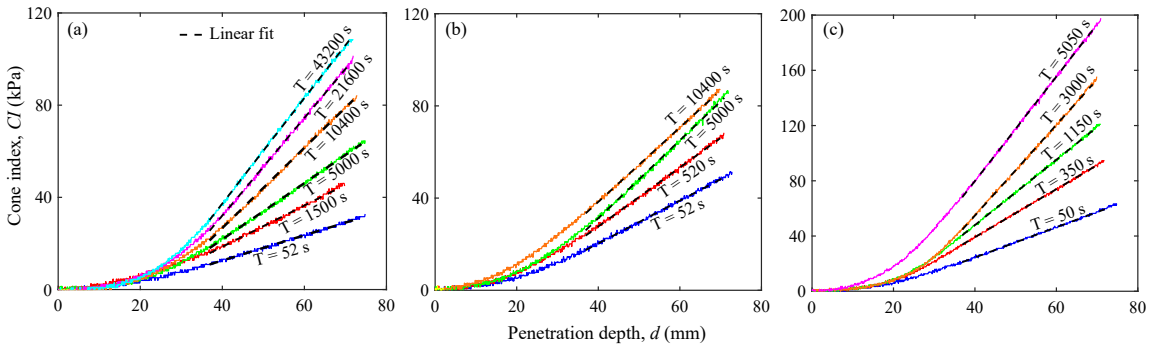

Figure 7: Cone index profiles of reconstituted beds prepared with various defluidization times for (a) *DO,* (b) *DFV,* and (c) *DCV.*

Fig. 7 presents plots of CI versus depth obtained at location O in the bed [see Fig. 4(b)]. The CI profiles become steeper with increasing T for all defluidization modes and differ between modes for the same T. In all cases, CI increases linearly with depth in the shaft penetration regime.

Soil density can be determined as a function of CI [43, 44, 45]. In the shaft penetration regime (cone fully submerged), the linear relation between CI and depth indicates a uniform density [46]. The slope of the cone index curve, G, can be directly related to density [45]:

$$\rho = a \ln(G/b), \tag{4}$$

where a and b are constants dependent on soil type.

To determine the bed density from G, constants a and b from Eq. (4) must be found. To do so, cone penetration tests were performed on 150 mm deep pluviated samples of known density in a cylindrical container (diameter = 200 mm). Different sample densities were achieved by varying the pluviator hole size and the uniform grid spacing of the holes (2 mm holes spaced by 25 mm, 4 mm holes spaced by 20 mm, and 6 mm holes spaced by 20 mm) and by placing the pluviator at various heights (15.2 cm, 30.5 cm, 71.0 cm, and 91.5 cm) above the soil surface. The penetrometer was inserted along the central axis of the cylindrical container, and at least three samples were prepared and tested at the same nominal density. By fitting the data to Eq. (4) as shown in Fig. 8(a),

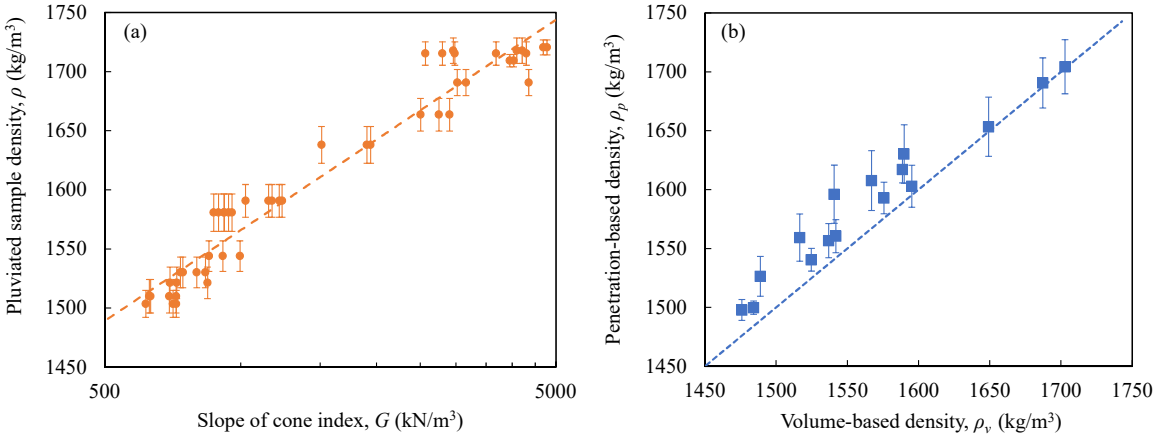

Figure 8: (a) Volume-based densities vs. dimensionless slopes of cone index curve for samples prepared by pluviation. Dashed line is a fit to Eq. (4) and is used to determine fit parameters a and b (see text). (b) Comparison of volume-based and penetration-based density measurements for various defluidization rates and modes.

the constants a and b of the calibration curve were determined to be $110.6\,\mathrm{kg/m^3}$ and $7.1 \times 10^{-4}\,\mathrm{kN/m^3}$, respectively with $R^2 = 0.94$. Using the calibration equation [Eq. (4)] and the slope of the cone index curve, local densities can be calculated at any location in the bed.

To validate the penetrometer-based approach, the volume-based and penetrometer-based bed densities of various reconstituted sand beds are compared in Fig. 8(b). The penetrometer-based density (ρ_p) is the mean of the densities obtained from the 21 bed positions, and the volume-based density (ρ_v) is determined as described in the section entitled "Volumetric density." The penetrometer-based densities are in good agreement with the volume-based values (coefficient of determination $R^2 = 0.78$), indicating that the sand density in the bed is reliably determined using the calibration curve. Note that the penetrometer-based densities are slightly larger than the volume-based values for $\rho_v < 1600\,\mathrm{kg/m^3}$, and that the reason for this discrepancy is not yet understood.

3.2.2. Density variation with depth

To characterize possible variation in bed density with depth, we examine the linearity of the cone-index profiles in the shaft-penetration regime (see Fig. 6). Typical cone index profiles [obtained at location O in the bed, see Fig. 4(b)] are presented in Fig. 7 and appear to be quite linear in the shaft-penetration regime. To quantify any possible variation, a linear regression is performed on the data in the shaft penetration regime for the three defluidization modes and various times, and the coefficient of determination (R^2) is calculated. R^2 values are determined at all 21 sampling locations, and the minimum values (worst case) are presented in Table 1. The smallest value of R^2 for all sampling locations, all defluidization modes, and all defluidization times is 0.982, which indicates that variation of density with depth is negligible.

3.2.3. Density variation across the bed

Having shown that density variation with depth is minimal, we now examine spatial variation across the bed. To quantify spatial variation, spatially averaged values and standard deviations (SD) of the slope of the cone index curve (G), density (ρ_p), and relative density (D_r) are listed in Table 1. The coefficients of variation of density (COV_{ρ_p}) and relative density (COV_{D_r}) are also provided, where $COV_X = SD_X/\overline{X}$ for variable X. COV_{D_r} values are less than 13% except for beds prepared by DO at intermediate $\overline{D_r}$. Beds prepared by DO with short T exhibit the smallest $\overline{D_r}$ where they also show small COV_{D_r}; DFV mode prepared beds have $0.3 \leq \overline{D_r} \leq 0.7$ with a small variation of density; for sand beds with $\overline{D_r} > 0.7$, the variation of density is slight when DCV is applied.

The data in Table 1 show that density variations across sand beds prepared by fluidization are relatively small. However, there is some spatial correlation in density variations as shown in Fig. 9-11 for beds prepared with various defluidization times using DO, DFV, and DCV, respectively. These contours are obtained by spline interpolation (MATLAB function interp2) of the densities at the 21 sampled locations.

For DO (Fig. 9), the highest density of sand appears in two isolated zones located

Table 1: Uniformity of sand samples prepared with three defluidization modes and various defluidization times.

Mode	Defluidization time, T[s]	Uniformity in depth	Uniformity across breadth				
		$R^2_{\min}$	Slope of cone index curve, $\overline{G} \pm \text{SD}[\text{kN/m}^3]$	Density, $\overline{\rho_p} \pm \text{SD}$ $[\text{kg/m}^3]$	COV_{ρ_p} [%]	Relatively density, $\overline{D_r} \pm \text{SD}$	COV_{D_r} [%]
DO	52	0.987	551±28	1499.72±5.70	0.38	0.20±0.02	11.4
	1500	0.984	707±105	1526.28±16.93	1.11	0.30±0.07	21.6
	5000	0.989	957±166	1559.23±20.06	1.29	0.43±0.07	17.4
	10400	0.991	1346±299	1596.03±24.69	1.55	0.56±0.09	15.5
	21600	0.992	1498±346	1607.67±25.40	1.58	0.60±0.09	14.7
	43200	0.993	1832±409	1630.10±24.85	1.52	0.68±0.08	12.4
DFV	52	0.991	798±68	1540.42±9.65	0.63	0.36±0.04	10.2
	520	0.982	960±121	1560.44±14.06	0.90	0.43±0.05	12.0
	5000	0.993	1286±157	1592.83±13.35	0.84	0.55±0.05	8.58
	10400	0.993	1596±162	1616.97±11.30	0.70	0.64±0.04	6.13
DCV	50	0.992	928±118	1556.67±14.48	0.93	0.42±0.05	12.9
	350	0.992	1415±227	1602.82±17.86	1.11	0.59±0.06	10.7
	1150	0.995	2259±479	1653.32±25.14	1.52	0.76±0.08	11.0
	3000	0.998	3143±581	1690.57±21.26	1.26	0.88±0.07	7.67
	5050	0.997	3567±684	1704.31±22.96	1.35	0.92±0.07	7.82

on opposite sides of the shorter bed midline. From these two peak zones, the density of sand decreases approximately radially. The lowest density is generally found in an area on the left side of the bed (as presented in the figure). Additionally, the density variation in the bed is not symmetric, which might be caused by the momentum of the air exiting the duct. Under this operating mode, the spatial uniformity of the sand bed can be improved by more uniformly distributing the air across the granular bed. For homogenizing the air distribution, the fluidized bed described in this paper can be refined in three ways: (1) increase the height of the plenum and the diameter of the plenum duct inlet to make air distribute more uniformly beneath the distributor; (2) increase the length of the vertical duct segment connecting to the plenum to reduce the asymmetric density distribution caused by the momentum of the air flowing from the duct; (3) use a distributor with higher resistance to reduce flow variation by creating a higher pressure drop, which can be realized by either increasing the thickness or reducing the pore size of the distributor.

For *DFV* (Fig. 10), relatively high density is observed to the left of the bed center, and the density mostly decreases gradually towards the left and right. Overall, the density on the left side of the bed is higher than on the right side. Additionally, the density of sand is higher toward the near side of the bed (smaller y coordinates). For *DCV* (Fig. 11), the density distribution of sand is similar to that of *DFV*. The density is high at the center of the bed and decreases gradually towards the left and right. Note that the density is higher on the far side of the bed (larger y coordinates) which is the reverse of the case for *DFV*. This variation likely results from the position of the vibration source at one side of the middle of the fluidized bed's frame (see Fig. 1). Compared to the result of *DO*, it is observed that vibration has a significant influence on the densification of a sand bed. By varying the attachment position(s) of the vibrator(s), one can obtain different density distributions of the bed. Hence, more vibrators can be added to the bed with a rational arrangement to reconstitute the sand bed more uniformly.

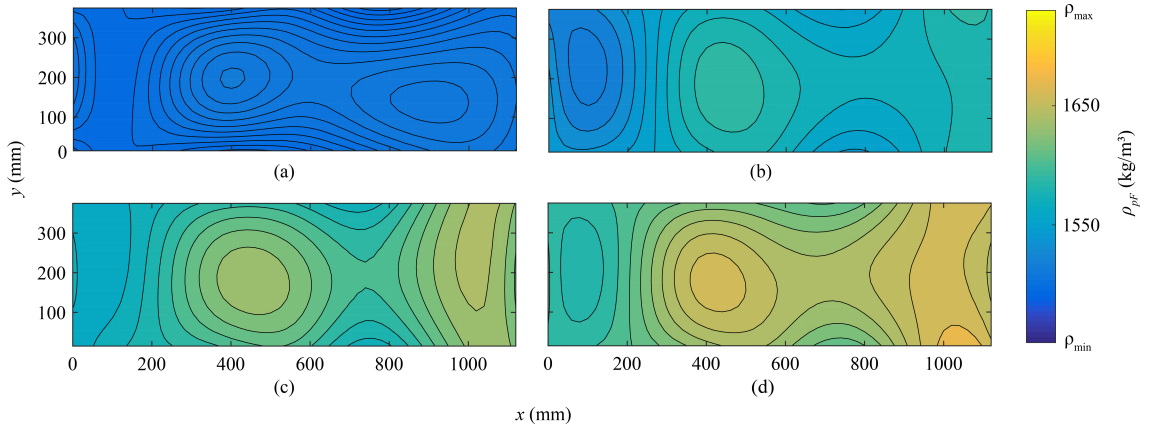

Figure 9: Density distribution across sand beds prepared by *DO* with defluidization times T of (a) 52 s ($\boldsymbol{COV_{\rho_p} = 0.38\%}$); (b) 5000 s ($\boldsymbol{COV_{\rho_p} = 1.29\%}$); (c) 10400 s ($\boldsymbol{COV_{\rho_p} = 1.55\%}$); and (d) 43200 s ($\boldsymbol{COV_{\rho_p} = 1.52\%}$).

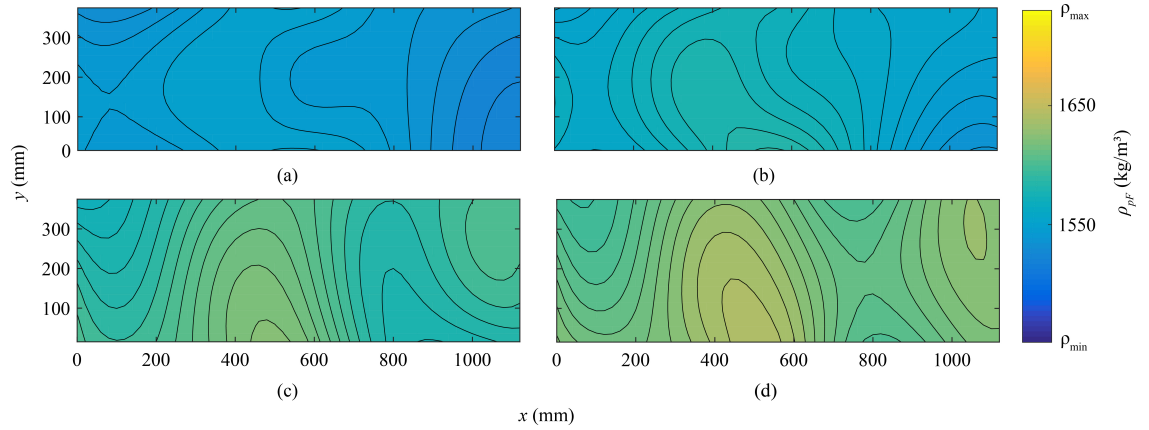

Figure 10: Density distribution across sand beds prepared by *DFV* with defluidization times T of (a) 52 s ($\boldsymbol{COV_{\rho_p} = 0.63\%}$); (b) 520 s ($\boldsymbol{COV_{\rho_p} = 0.90\%}$); (c) 5000 s ($\boldsymbol{COV_{\rho_p} = 0.84\%}$); and (d) 10400 s ($\boldsymbol{COV_{\rho_p} = 0.70\%}$).

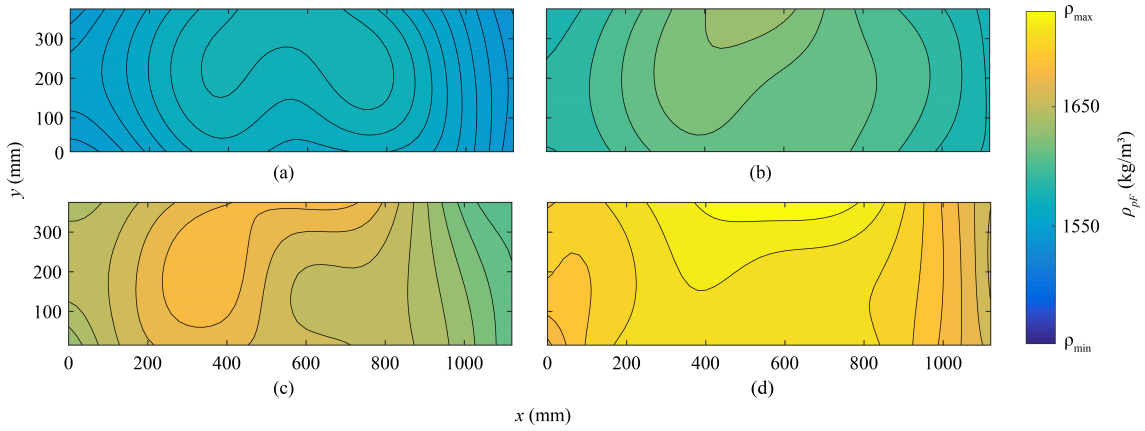

Figure 11: Density distribution across sand beds prepared by DCV with defluidization times T of (a) 50 s ($\boldsymbol{COV_{\rho_p} = 0.93\%}$); (b) 350 s ($\boldsymbol{COV_{\rho_p} = 1.11\%}$); (c) 1150 s ($\boldsymbol{COV_{\rho_p} = 1.52\%}$); and (d) 5050 s ($\boldsymbol{COV_{\rho_p} = 1.35\%}$).

4. Equivalence of beds prepared by fluidization and pluviation

To show that pluviated beds and beds prepared by fluidization are equivalent, Fig. 12 compares the dependence of the penetration-based density ρ_p in beds prepared by fluidization to those prepared with pluviation as a function of the slope of the cone index curve G. ρ_p and G are averages of measurements performed at the 21 sample locations and are given in Table 1. The horizontal error bars represent the standard derivation of G at the different average densities, and the vertical error bars represent the standard derivation of ρ_p at various $\overline{G}$. Error bars illustrate the variations of the corresponding quantities. Gray data points are from samples prepared by pluviation, and each data point represents the result from one test. The figure indicates that the density variations and G for beds prepared by fluidization are within the range of the results from the widely used pluviation method, suggesting that fluidized beds are capable of reconstituting sand beds for geotechnical modeling tests.

5. Conclusions

This paper explores the application and demonstrates the suitability of air-fluidization for reconstituting sand beds for geotechnical modeling tests. Details of the device and

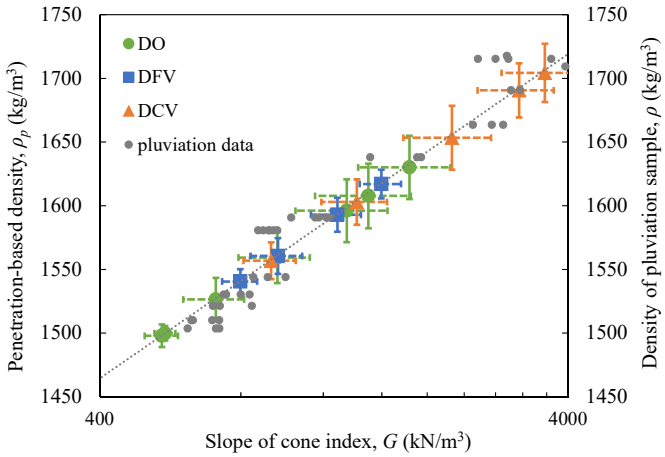

Figure 12: Bed density vs. cone index curve slope across sand beds prepared by fluidization (colored symbols) and pluviation (gray circles) indicates equivalence of the two bed reconstitution techniques (see text).

the design methodology are presented along with the capabilities of the fluidized bed device, which provides a reference for future applications of this method. Through the study of volumetric densities and local densities across the beds, sand beds reconstituted using three different operating modes (*DO*, *DFV* and *DCV*) and with various defluidization times are characterized, and the performance of the fluidized bed device is evaluated. The main conclusions are as follows:

(i) Sand beds can be prepared with a broad range of volume-based relative density from 10.4% to 91.7% by using the three operating modes and corresponding pressure ramp rates illustrated in this study. For *DO*, *DFV* and *DCV*, the relative densities realized are 10.4% - 54.1%, 27.6% - 53.7%, 34.6% - 91.7%, respectively. These ranges can be further expanded by extending the bounds of the pressure ramp rates used here.

(ii) The sand bed is nearly spatially homogeneous based on cone penetration measurements. Along the depth, minimum R^2 values are close to 1 for all beds prepared by the three modes with different pressure ramp rates, indicating that their density variations with depth are minimal. Across the breadth of the bed, the coefficients of variation of relative density are found to be under about 13% for all beds except

for some prepared by *DO*. In addition, by correlating penetration measurements to local densities, the result also serve as a more direct reflection of the fact that the mechanical properties of sand beds are uniform given that the critical features of the cone index profiles across each bed show little variation.

(iii) A fluidized bed is qualified for reconstituting sand beds for geotechnical modeling tests given that the beds prepared by fluidization and the widely used method pluviation are comparable. The latter is inferred from the fact that the density variations and slopes of the cone index for beds prepared by fluidization are within the range of the results obtained using the pluviation method.

(iv) The application of air fluidization is not confined to the material and bed dimensions used in this study. Fluidized bed devices are capable of being used in various types of geotechnical modelling tests with different soil properties and bed sizes.

6. Acknowledgements

We thank Sam Asa and Olisaeloka Anazonwu for their assistance in the experiments related to pluviation. This material is based upon work supported by the National Science Foundation under Grant No. CMMI 1742849.

References

[1] N. Meyer, A. Nernheim, U. Köhler, Geosynthetic-soil interaction under cyclic loading, in: 3rd European Geosynthetics Conference, Munich, Germany, Vol. 103, 2004, pp. 635–639.

[2] G. Gottardi, G. Houlsby, R. Butterfield, Plastic response of circular footings on sand under general planar loading, Géotechnique 49 (4) (1999) 453–470.

[3] R. Butterfield, K. Andrawes, An air activated sand spreader for forming uniform sand beds, Géotechnique 20 (1) (1970) 97–100.

[4] S. Miura, S. Toki, A sample preparation method and its effect on static and cyclic deformation-strength properties of sand, Soils and foundations 22 (1) (1982) 61–77.

[5] M. El Sawwaf, A. K. Nazir, Behavior of repeatedly loaded rectangular footings resting on reinforced sand, Alexandria Engineering Journal 49 (4) (2010) 349–356.

[6] M. Raghunandan, A. Juneja, B. Hsiung, Preparation of reconstituted sand samples in the laboratory, International Journal of Geotechnical Engineering 6 (1) (2012) 125–131.

[7] C. Chen, Q. Quan, Z. Deng, S. Jiang, Vibratory compaction method for preparing lunar regolith drilling simulant, Advances in Space Research 58 (1) (2016) 145–154.

[8] B. W. Byrne, Investigations of suction caissons in dense sand, Ph.D. thesis, University of Oxford Oxford, UK (2000).

[9] D. White, A. Barefoot, M. Bolton, Centrifuge modelling of upheaval buckling in sand, International Journal of Physical Modelling in Geotechnics 1 (2) (2001) 19–28.

[10] K. Miura, K. Maeda, M. Furukawa, S. Toki, Mechanical characteristics of sands with different primary properties, Soils and Foundations 38 (4) (1998) 159–172.

[11] D. L. Presti, S. Pedroni, V. Crippa, Maximum dry density of cohesionless soils by pluviation and by ASTM D 4253-83: A comparative study, Geotechnical Testing Journal 15 (2) (1992) 180–189.

[12] B. Walker, T. Whitaker, An apparatus for forming uniform beds of sand for model foundation tests, Geotechnique 17 (2) (1967) 161–167.

[13] T. N. Dave, S. Dasaka, Assessment of portable traveling pluviator to prepare reconstituted sand specimens, Geomechanics and Engineering 4 (2) (2012) 79–90.

[14] C. Fretti, D. L. Presti, S. Pedroni, A pluvial deposition method to reconstitute well-graded sand specimens, Geotechnical testing journal 18 (2) (1995) 292–298.

[15] C. Hariprasad, M. Rajashekhar, B. Umashankar, Preparation of uniform sand specimens using stationary pluviation and vibratory methods, Geotechnical and Geological Engineering 34 (6) (2016) 1909–1922.

[16] B. Maillot, A sedimentation device to produce uniform sand packs, Tectonophysics 593 (2013) 85–94.

[17] Y. P. Vaid, D. Negussey, Relative density of pluviated sand samples, Soils and Foundations 24 (2) (1984) 101–105.

[18] N. S. Rad, M. T. Tumay, Factors affecting sand specimen preparation by raining, Geotechnical Testing Journal 10 (1) (1987) 31–37.

[19] J. Kolbuszewski, An experimental study of the maximum and minimum porosities of sands, in: Proceedings of the 2nd international conference on soil mechanics and foundation engineering, Rotterdam, Vol. 1, 1948, pp. 158–165.

[20] Y. Vaid, D. Negussey, Preparation of reconstituted sand specimens, in: Advanced triaxial testing of soil and rock, ASTM International, 1988.

[21] F. Qian, D. I. Goldman, The dynamics of legged locomotion in heterogeneous terrain: universality in scattering and sensitivity to initial conditions., in: Robotics: Science and Systems, 2015, pp. 1–9.

[22] F. Qian, T. Zhang, W. Korff, P. B. Umbanhowar, R. J. Full, D. I. Goldman, Principles of appendage design in robots and animals determining terradynamic performance on flowable ground, Bioinspiration & biomimetics 10 (5) (2015) 056014.

[23] C. Li, P. B. Umbanhowar, H. Komsuoglu, D. E. Koditschek, D. I. Goldman, Sensitive dependence of the motion of a legged robot on granular media, Proceedings of the National Academy of Sciences 106 (9) (2009) 3029–3034.

[24] C. Li, S. T. Hsieh, D. I. Goldman, Multi-functional foot use during running in

the zebra-tailed lizard (callisaurus draconoides), Journal of Experimental Biology (2012) jeb–061937.

[25] C. Li, T. Zhang, D. I. Goldman, A terradynamics of legged locomotion on granular media, Science 339 (6126) (2013) 1408–1412.

[26] R. D. Maladen, Y. Ding, C. Li, D. I. Goldman, Undulatory swimming in sand: subsurface locomotion of the sandfish lizard, science 325 (5938) (2009) 314–318.

[27] P. Umbanhowar, D. I. Goldman, Granular impact and the critical packing state, Physical Review E 82 (1) (2010) 010301.

[28] D. Geldart, Types of gas fluidization, Powder technology 7 (5) (1973) 285–292.

[29] D. Geldart, A. R. Abrahamsen, Homogeneous fluidization of fine powders using various gases and pressures, Powder Technology 19 (1) (1978) 133–136.

[30] Z. Yang, Y. Tung, M. Kwauk, Characterizing fluidization by the bed collapsing method, Chemical Engineering Communications 39 (1-6) (1985) 217–232.

[31] S. Ergun, Fluid flow through packed columns, Chem. Eng. Prog. 48 (1952) 89–94.

[32] F. Blake, The resistance of packing to fluid flow, Transactions of the American Institute of Chemical Engineers 14 (3) (1922) 415–421.

[33] S. P. Burke, W. Plummer, Gas flow through packed columns1, Industrial & Engineering Chemistry 20 (11) (1928) 1196–1200.

[34] J. Wu, B. Yu, M. Yun, A resistance model for flow through porous media, Transport in Porous Media 71 (3) (2008) 331–343.

[35] I. Gasho, Blower application basics, Website, last checked: 06.09.2019 (8 2009). URL https://www.gasho.org/wp-content/uploads/Blower-Application-Basics.pdf

[36] F. Zenz, Bubble formation and grid design, in: Institution of Chemical Engineers Symposium Series, 1968, pp. 136–139.

[37] D. Geldart, J. Baeyens, The design of distributors for gas-fluidized beds, Powder Technology 42 (1) (1985) 67–78.

[38] ASTM:D4253-16, Standard test methods for maximum index density and unit weight of soils using a vibratory table, ASTM International, West Conshohocken, PA.

[39] ASTM:D4254-16, Standard test methods for minimum index density and unit weight of soils and calculation of relative density, ASTM International, West Conshohocken, PA.

[40] N. Brady, R. Weil, Organisms and ecology of the soil, in: Nature and Properties of Soil, Vol. 11, Prentice Hall, Upper Saddle River, New Jersey, USA, 1996, pp. 328–360.

[41] N. Gravish, P. B. Umbanhowar, D. I. Goldman, Force and flow at the onset of drag in plowed granular media, Physical Review E 89 (4) (2014) 042202.

[42] WES, Trafficability of soils: Development of testing instruments, Tech. Rep. 3-240, U.S. Army Engineer Waterways Experiment Station, Vicksburg, MS (1965).

[43] P. Ayers, J. Perumpral, Moisture and density effect on cone index, Transactions of the ASAE 25 (5) (1982) 1169–1172.

[44] G. Pillinger, A. Géczy, Z. Hudoba, P. Kiss, Determination of soil density by cone index data, Journal of Terramechanics 77 (2018) 69–74.

[45] H. J. Luth, R. D. Wismer, Performance of plane soil cutting blades in sand, Transactions of the ASAE 14 (2) (1971) 255–0259.

[46] D. R. Freitag, A dimensional analysis of the performance of pneumatic tires on soft soils., Tech. Rep. 3-688, U.S. Army Waterways Experiment Station (1965).